

Modular and versatile platform for the benchmarking of modern actuators for robots

Elena Garcia* and Pablo Gonzalez-de-Santos

*Field and Service Robotics Group, Centre for Automation and Robotics -CSIC-UPM
28500 Madrid, Spain*

(Received July 28, 2011, Revised April 23, 2012, Accepted July 22, 2012)

Abstract. This work presents a test platform for the assessment and benchmarking of modern actuators which have been specifically developed for the new field and service robotics applications. This versatile platform has been designed for the comparative analysis of actuators of dissimilar technology and operating conditions. It combines a modular design to adapt to linear and rotational actuators of different sizes, shapes and functions, as well as those with different load capacities, power and displacement. This test platform emulates the kinematics of robotic joints while an adaptive antagonist-load actuator allows reproducing the variable dynamic loads that actuators used in real robotics applications will be subjected to. A data acquisition system is used for monitoring and analyzing test actuator performance. The test platform combines hardware and software in the loop to allow actuator performance characterization. The use of the proposed test platform is demonstrated through the characterization and benchmarking of three controllable impedance actuators recently being incorporated into modern robotics.

Keywords: benchmarking of actuators; experimental testing; test bench design; modular and versatile design; instrumentation; force control

1. Introduction

During the last 50 years, the evolution of robotics application fields and their sophistication have influenced research topics in the robotics community. This evolution has been dominated by human necessities. With the 21st century, the new trends in robotics research have been denominated field and service robotics (Garcia *et al.* 2007), because of their general goal of covering field applications such as agriculture, demining, search and rescue tasks; and service applications covering cleaning, construction, medical, rehabilitation and assistive applications such as robotic exoskeletons, active orthosis and prosthesis as a few examples, thus achieving the goal of getting robots closer to human social needs. The common challenge in the success of this new generation of robots is autonomy. Although some kinds of service robots work in place (i.e., medical and some rehabilitation robots), the general field-and-service robot is envisaged to move autonomously. Very few of this new generation of robots can benefit from the conventional actuation technology inherited from industrial robotics. There are five major challenges for

*Corresponding author, Dr., E-mail: elena.garcia@csic.es

developing functional field and service robots which are shown in Fig. 1. The primary challenge is that robots need to carry their own power source, thus increasing the overall payload to be moved by onboard actuators. A second challenge of the new generation of legged robots is the great amount of power needed by the actuators to feed the robot's mechanical power required for motion considering the payload. Because autonomous robots carry their own actuators, an increase of actuator weight would rely on an overall increase in robot weight, which in turn will require larger power for a given performance. Therefore, the only possible solution is to use large power-to-weight actuators.

Also, field and service robots interact with the environment and usually with humans. This is a feature completely different from industrial robotics, which always work enclosed apart from the human operator. Thus, robot-environment interaction schemes and safety play another key role in the emerging robotics research. Therefore, actuators for field and service robots should have low mechanical impedance or backdriveability to allow the robot's adaptation to the environment and to the human. Besides, compliance in actuators is desirable for minimizing shock and vibration effects during interaction with the environment, and for storing elastic energy in passive elastic elements to be released in the forthcoming phase of the locomotion cycle.

All, energy efficiency, high specific power, force controllability and low mechanical impedance requirements cannot be met with conventional actuator technology (Garcia *et al.* 2009a).

Considering this lack of adequate actuation systems for the new generation of robots for field and service applications, roboticists have started to research on new actuation technologies for the emerging robotics applications. This builds up a new research line on empowering technology for field and service robots, aimed at designing, developing and testing specific actuators and control schemes able to supply the power required at low weight and to provide energy-efficient robot motion.

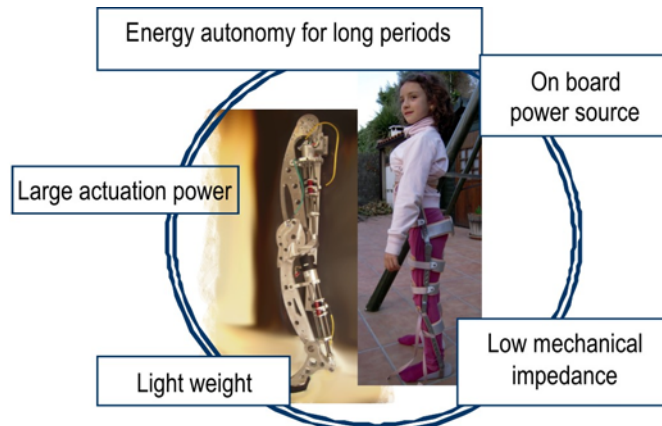


Fig. 1 Five challenges for the development of functional field and service robots

Series Elastic Actuators (SEAs) (Robinson 2000), Controllable-Stiffness Actuators (Ham *et al.* 2009, Hurst *et al.* 2010, Catalano *et al.* 2010) and Pneumatic Artificial Muscles (PAMs) (Klute and Hannaford 2000, Vanderborght *et al.* 2006) have been devised for achieving the goal of minimizing or adjusting the robot's mechanical impedance while improving the power-to-weight

ratio.

A parallel important research effort concentrates on the use of smart materials for the development of novel actuation systems (Song *et al.* 2011, Mahfoud and Der Hagopian 2012). Among the smart-material based actuators being developed, those approaching the field and service robot requirements are: Electroactive Polymers (EAPs) (Bar-Cohen 2000) and Ionic Polymer Metal Composite (IPMC) actuators (Çilingir and Papila 2010) as artificial muscles; Electrorheological fluids (ERF) and Magnetorheological fluids (MRF) (Mavroidis 2002, Carlson *et al.* 2004), which implement resistive devices; and Ferromagnetic Shape Memory Alloys (FSMA) (Suorsa *et al.* 2006; Pestana *et al.* 2010). The smart-material based actuator technology still features large power consumption to approach the goal of autonomy.

Currently, hybrid technology actuators are being explored that will meet the required characteristics by using a combination of the previously mentioned technologies and materials, with the goal of improving efficiency and satisfying the requirements of robotics. Examples are piezo-hydraulic (Anderson *et al.* 2003), piezo-pneumatic, MRF-SEA (Garcia *et al.* 2011b), and other combinations of smart materials and conventional technologies.

Taking into consideration that all these new actuator technologies are still in the stage of preliminary prototyping by a few researchers, there are no published catalogues or specifications that can help the interested roboticist in the selection of one or the other technology. The robotics researcher has little information to decide which actuator technology fits within his/her actuation requirements. Characterization and benchmarking of these emerging actuation technologies is needed.

In order to test, characterise and experimentally compare the performance of the new actuation mechanisms and drives, a versatile test bench is necessary, one that can accommodate linear and rotational actuators of different shapes, sizes, strains, and power (hydraulic, electric, pneumatic, piezoelectric, etc.). Likewise, it is important to reproduce the real working conditions that these actuators will be exposed to; hence, a suitable bench will generate and withstand high loads which are variable in time as well as vibrations. It must also be constituted correctly in order to monitor variables such as force, displacement, power and response time.

Conventional test-benches for characterising actuators are designed for a unique specific power technology (electrical, hydraulic, pneumatic) and recently very few test benches are able to test different motion types (linear, rotational) (Testek Inc. 2011). To these authors' best knowledge there is no commercially available test-bench able to adapt to such a wide range of actuator types and to allow their comparative analysis. Roboticists interested in analysing new actuators' performance need to use different test benches for each test actuator technology, and the dissimilar test conditions make it difficult to compare the results with appropriate rigor.

Besides, in order to validate the performance of an actuator, it is important to reproduce as realistically as possible the operating conditions of the test actuators inside robots. Actuators for robots do not perform in continuous mode, but they normally run cyclically at varying speeds, accelerating and decelerating a non-constant load, which comes from the non-linear dynamics of the robotic structure. Therefore, it is of poor interest for the roboticist to have an actuator being tested at constant speed and fixed load. In real robotic applications, actuators are subjected to non-linear functions of load. Therefore, some means to provide a programmable antagonist cyclic load function would be essential.

In this work, a versatile test platform for the comparative analysis of actuators is presented (Garcia *et al.* 2009b). The test platform is a modular chassis design able to adapt its geometry and operation conditions to the different technologies of the actuator to be tested. The platform

reproduces the kinematic operating conditions of actuators in robots by working to move a rotational axis like a robot rotational joint. The non-linear dynamics that are typical of a real robot are also reproduced in this test platform making use of a series-elastic hydraulic antagonist actuator which is force-controllable with high fidelity (Robinson and Pratt 2000). Section 2 describes the conceptual design of the proposed versatile test platform. Section 3 develops on the mechanical design. Section 4 describes the overall measurement and instrumentation setup, and Section 5 shows the force-control scheme for the antagonist programmable load actuator. Section 6 shows experimental characterization and benchmarking of actuators using the proposed test bench and finally Section 7 presents some conclusions.

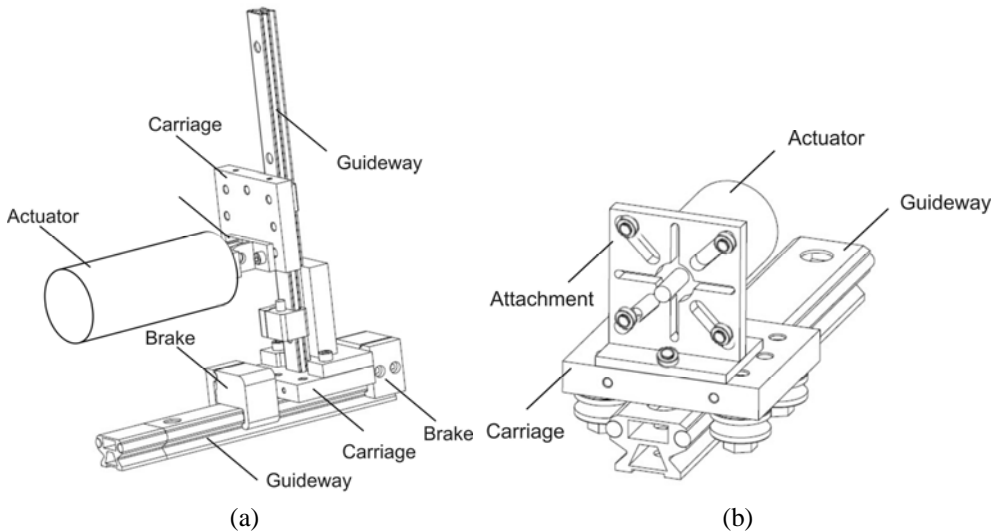


Fig. 2 Attachment of actuators to carriages: (a) Linear actuators attach to vertical carriages and (b) rotational actuators attach to horizontal carriages by means of a special attachment element which consists of eight grooves that can house actuators of different diameter, different axis diameter, and different screw size and pitch circle diameter

2. Modular and versatile concept

The proposed test platform is based on a reconfigurable chassis composed of removable modules which allow the platform to be adapted to the test actuator technology, size, and operational conditions. The set of removable modules consists mainly of:

1. A test actuator, which can be either linear or rotational;
2. A central axis transmission system (emulating a robot rotational joint);
3. A sensorial unit which provides measurement of torque, joint speed and joint angle;
4. An antagonist load actuator, which can be either linear or rotational; and
5. A removable climate chamber, which is used only when special temperature conditions are required for the test.

The reconfigurable chassis is based on four linear guideways attached to a rectangular base.

Four carriages slide on the linear guideways. The carriage and guideway of a linear recirculating roller bearing and guideway assembly, shown in Fig. 2, are matched to each other as a low-friction standard system due to their closely toleranced preload. Linear recirculating roller bearing and guideway assemblies are suitable for high and very high loads. The linear motion of the carriages can be blocked making use of brakes at the desired position in order to fit with the size of the actuators. Each carriage can be connected to a vertical guideway with carriage. Each linear actuator is connected to a vertical carriage (see Fig. 2(a)), while rotational actuators are attached to horizontal carriages axially aligned with the central axis transmission system (see Fig. 2(b)). The chassis can be configured for each type of actuator by selecting a guideway and adjusting the carriage to the actuator size. The remaining mobile parts can be connected to the base of the chassis in different positions, being able to reconfigure four different chassis geometries for the following four operational modes:

1. **Linear-linear operational mode** (Fig. 3(a)): The test actuator is linear and the antagonist actuator is linear. Therefore the chassis is configured in a way that both actuators are connected to the central axis through connecting rods (see Fig. 4(a)). In order to measure the torque and rotational motion exerted to the load, the sensorial unit is placed between both connecting rods. The test actuator and the antagonist actuator are connected to the chassis through each mobile carriage. In this operational mode, the test actuator makes torque to the central axis through the rod moment arm while the antagonist actuator exerts the programmed load function through the rod moment arm.
2. **Linear-rotational operational mode** (Fig. 3(b)): The test actuator is linear and the antagonist actuator is rotational. Therefore, the linear test actuator is connected to the central axis through a connecting rod (see Fig. 4(a)) and the antagonist rotational actuator is connected to the central axis through elastic couplings (see Fig. 4(b)). The chassis fits to the actuators size through mobile carriages. The test actuator makes torque to the central axis through the rod moment arm, while the antagonist rotational actuator exerts the programmed load function through direct rotational torque.
3. **Rotational-linear operational mode** (Fig. 3(c)): The test actuator is rotational and the antagonist actuator is linear. The rotational test actuator is connected to the central axis through elastic couplings (see Fig. 4(b)) and the linear antagonist actuator is connected to the central axis through a connecting rod (see Fig. 4(a)). The chassis fits to the actuators size through mobile carriages. The rotational test actuator is connected to the mobile carriage through a special attachment shown in Fig. 2(b) which allows to connect actuators of different diameter, different axis diameter, and different screw size and pitch circle diameter. Then, the rotational test actuator exerts direct rotational torque while the antagonist actuator exerts the programmed load function through the rod moment arm.
4. **Rotational-rotational operational mode** (Fig. 3(d)): The test actuator is rotational and the antagonist actuator is rotational. Both actuators transmit rotational torque to the central axis through elastic couplings (see Fig. 4(b)). The rotational test actuator is connected to the mobile carriage through a special attachment shown in Fig. 2(b) which allows to connect actuators of different diameters. The antagonist rotational actuator exerts the programmed load function through direct rotational torque.

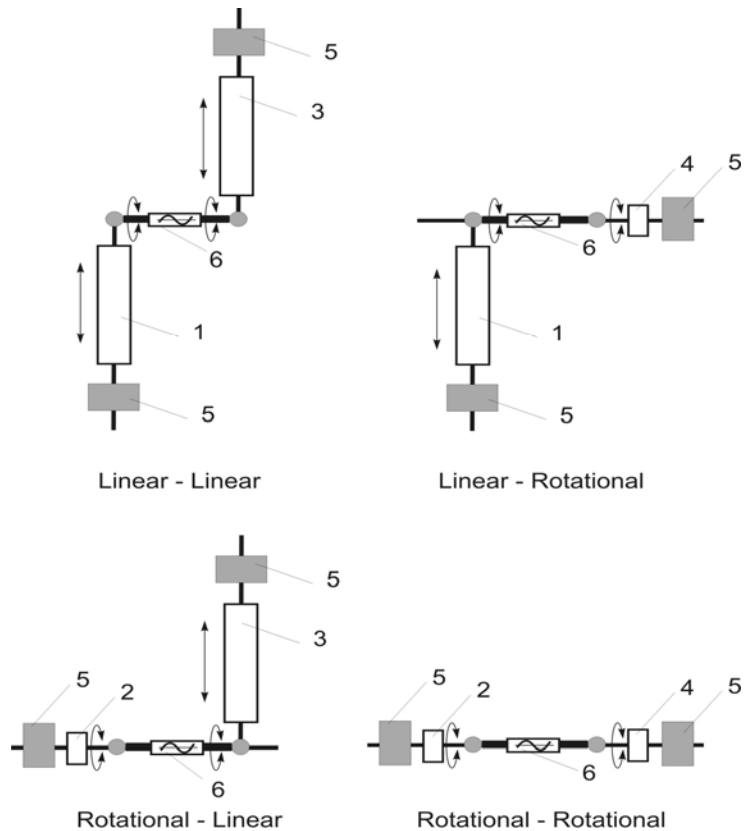


Fig. 3 Four operational modes of the test platform. Legend: 1- Linear test actuator; 2- Rotational test actuator; 3- Linear antagonist actuator; 4- Rotational antagonist actuator; 5- Mobile carriage; 6- Sensorial unit in the central axis.

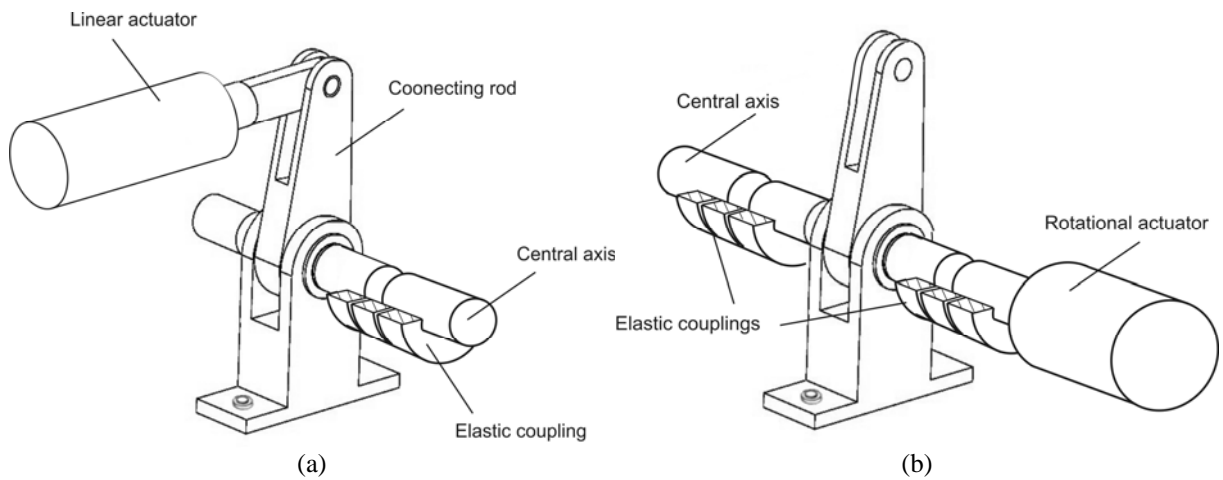


Fig. 4 Transmission of mechanical power between actuators and central axis: (a) Linear actuator is connected through connecting rod and (b) rotational actuator is connected through elastic couplings

The selection of one of these four operational modes will depend on the type of actuator to be tested, and on the force/torque capacity of the test actuator. For test actuators with very large maximum torque, the linear antagonist actuator will be used because of its capability of applying larger torques through the rod moment arm. The definition and operation of the sensorial unit located in the central axis will be presented in Section 4. Figure 5 shows a 3D-view of the test platform in Linear-linear operational mode.

3. Mechanical design

This section aims to justify the decisions and considerations that were kept in mind in order to define the dimensions and characteristics of each of the elements that are used in the versatile test platform. After clarifying limitations, establishing design criteria and identifying the characteristics of the actuators that are intended to be tested, a preliminary outline was performed with a parametric, integrated 3D CAD/ CAM/ CAE application (PTC, 2007) to determine which elements should be used in the bench, and how to position them to achieve the desired versatility, as well as which and how many pieces needed to be manufactured or bought. Equations were also obtained in this part, which, with the designed configuration, determine the kinematics and dynamics of the system, and are also used for the calculation of the actuators' variables to be identified. The derivation of these equations of motion is detailed in the Appendix. Later, a detailed design was created using the same software. This consisted both in performing an analysis of forces and fatigue, as well as assembling and preparing the bench, simulating its operation to evaluate the arrangement, comfort and adjustment of the elements, guaranteeing compliance with the previously mentioned design criteria. Later, the production plans for the necessary pieces were created.

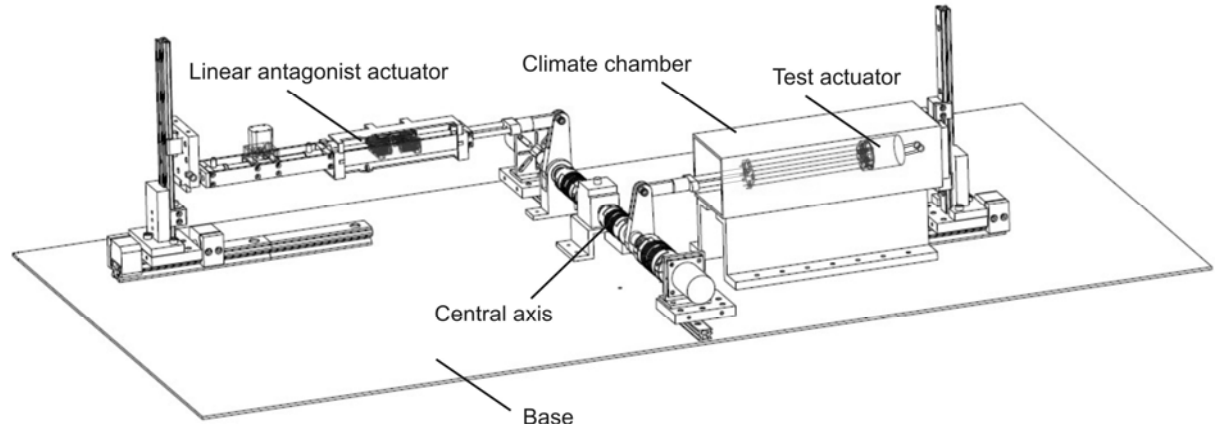


Fig. 5 3D-view of the test platform in Linear-linear operational mode

The design limitations involved those considerations that represent imposed, invariable conditions for the bench design, due to the availability of equipment and the expected working

conditions of the test platform. Therefore, the bench's configuration and the selection of structural elements and main components such as the antagonist load actuators, the torque sensor and the flexible couplings depend on the magnitude of the variables to be measured.

The test platform aims to serve as a bench for the benchmarking of new actuators for robots. The magnitudes to be compared and analyzed for the tested actuators are: torque, speed, power, and efficiency. The specifications of the test actuators define the limits of these magnitudes, which are:

Linear test actuators:

- Maximum stroke: 200 mm
- Minimum stroke: 5 mm
- Maximum force: 2500 N
- Maximum speed: 1.5 m/s
- Maximum length: 650 mm including actuator stroke.

Rotational test actuators:

- Maximum torque: 200 Nm
- Maximum shaft diameter: 15 mm
- Minimum pitch circle diameter of attaching screws: 12 mm
- Maximum pitch circle diameter of attaching screws: 64 mm

The mechanical considerations that were kept in mind for the design, specification and manufacturing of the test bench elements and materials are specified below:

- Minimum distances and sizes to guarantee ease while installing/removing the actuators and adjusting the elements
- Maximum forces under the material's yield strength, divided by a safety factor of 1.5 to ensure resistance to dynamic loading.
- Fatigue life greater than 10^6 cycles
- Few mobile elements to prevent vibration

Having the dimensions of the actuators to be tested, and the magnitude of the variables to be measured in mind, resistance and distance criteria were established to ensure the bench's efficient operation.

Fig. 6 shows the assembled test platform configured in the linear-linear operational mode testing a pneumatic muscle.

4. Instrumentation, measurement and processing

4.1 Variables and sensors

As previously mentioned, the versatile test platform is intended to test, characterize and comparatively analyze the operation of linear or rotational actuators of any technology. In order to perform such an analysis, magnitudes of force, stroke, power, frequency and efficiency need to be

acquired during the tests. Bearing in mind that the bench is designed in such a way that any type of test actuator, linear or rotational, directly induces movement to the central rotational axis with only one degree of freedom, a sensor system able to measure static and dynamic torque and speed transmitted to the central axis would provide all the information required for the comparative analysis of actuators. As such, one dynamic sensor measuring nominal torques of 200 Nm and one position sensor measuring nominal rotation speeds of 3000 rpm is enough to define all of the variables that the user wishes to identify. The sensorial unit is mechanically connected to the platform's central axis by means of two bellows couplings that correct shaft misalignments (see Fig. 6). An intermediate terminal box is used to electrically connect the torque transducer to the data acquisition system. The equations of motion that relate the measured variables with the actuator variables are detailed in the Appendix.

In our test platform prototype, an HBM torque sensor model T20WN was used. This torque transducer's operational principle is based on measuring the small torsional elastic strains on the axis or rotor using strain gauges, which provides highly precise measurements. The measurement mechanism for the rotation angle and velocity consists of an optical encoder. After installing the transducer in the test platform, the torque sensor was calibrated.

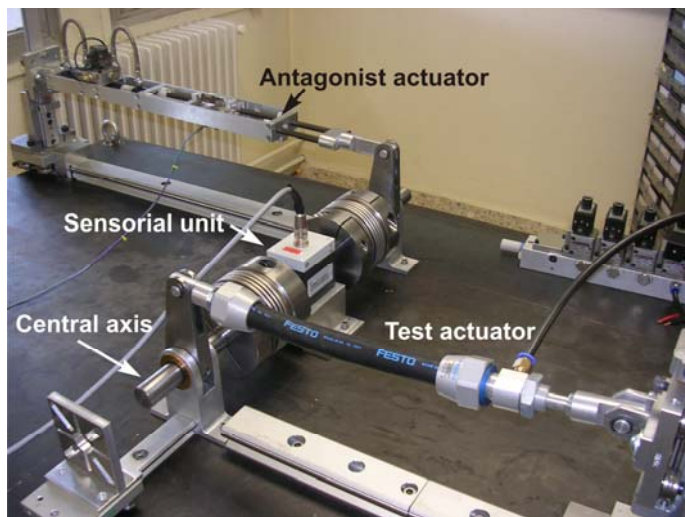


Fig. 6 Assembled test platform in Linear-linear operational mode

4.2 Data acquisition

To process the data provided by the sensor, a National Instruments PXI-1024Q industrial acquisition and control platform is used. This platform has an embedded controller running a Real Time operating system, and a NI PXI-6259 acquisition card. The software developed for the characterization, testing, and comparative analysis performed in the versatile test platform has been programmed using NI LabView. The developed application allows for the collection of data provided by the T20WN torque sensor and then displays the data on the screen or stores it in a text file. The graphical interface can display the torque magnitude, angle, velocity and power in real

time; it also displays its average and peak values. Additionally, all of this information can be stored in table form in a file for evaluation at a later point.

This acquisition system allows the user to perform the appropriate checks to test the actuators and to reproduce and vary the real dynamic conditions to which they would be subjected. Likewise, additional instrumentation can be connected and all of the information can be concentrated in digital format in just one computer.

5. Testing control

A main characteristic of the herein presented versatile test platform is the capability to reproduce the actuator's real work conditions during the test. The real work conditions are simulated by changing the environment's temperature, reproducing the actuator's kinematics, and generating antagonist dynamic loads.

The environment's temperature is modified by means of a climate chamber, which is removable. A thermocouple inside the chamber senses the temperature inside which is acquired making use of the data acquisition platform described above. The difference between the desired chamber temperature and the measured temperature is minimized by a Proportional - Integral - Derivative PID controller, whose output commands current to an electrical resistance to raise the chamber temperature. A fan helps in distributing the heat uniformly.

The kinematic work conditions are reproduced through the connecting rod - central axis set. The central axis acts as a robotic 1-DOF joint, actuated by a linear actuator through the connecting rod, or by a rotational actuator directly attached to the joint shaft.

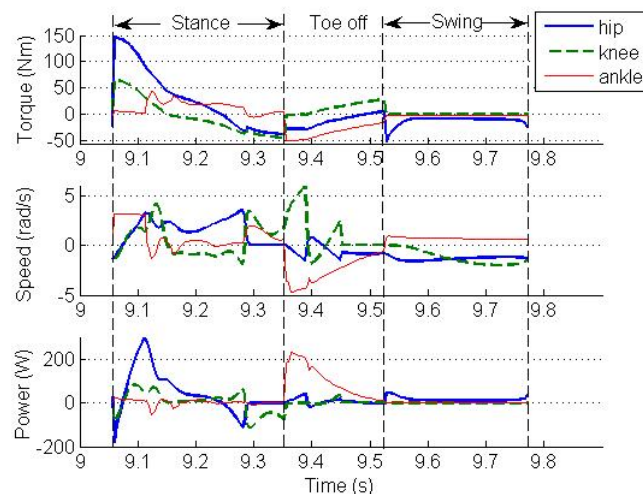


Fig. 7 Requirements of torque, speed and power for the joints of a robotic leg running at 1.5 m/s carrying a 12kg load in a locomotion cycle

The dynamic work conditions of the actuators of robots are torque functions that repeat cyclically. The torque, speed and power required at the hip, knee and ankle joints of a 5-kg 1m-

long robotic leg walking at 1.5 m/s while carrying a 12 kg payload above its hip are shown in Fig. 7 for one gait cycle. It can be observed how the torque function is not constant but sharply variable along the phases of robot motion. These abrupt variations of the torque function are due to the coupled limb inertia, centrifugal joint velocities, gravitational forces, and ground interaction forces involved in the robot's dynamics.

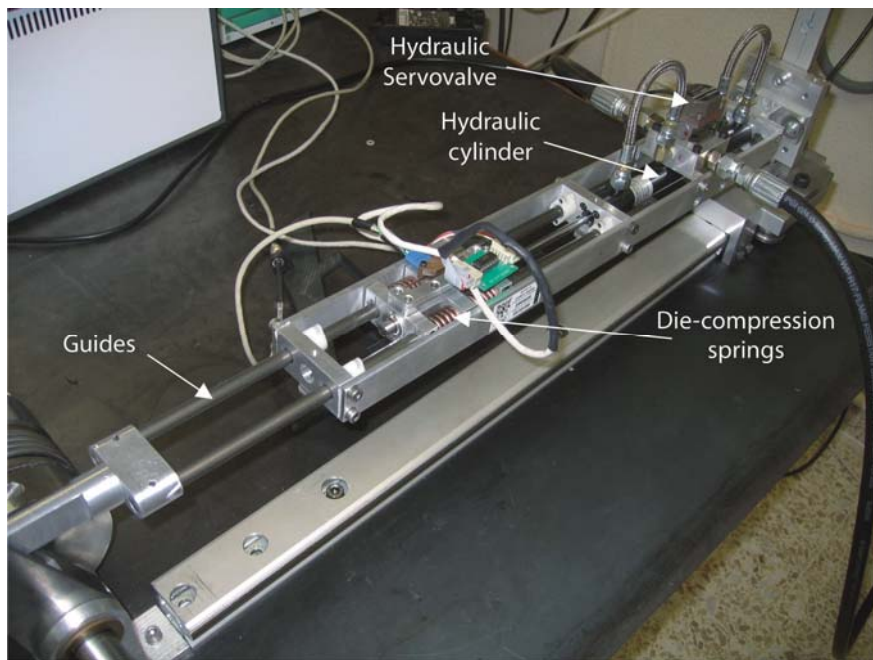


Fig. 8 Antagonist load actuator

In order to reproduce these dynamic work conditions, a force-programmable hydraulic antagonist actuator has been proposed which belongs to the family of Series Elastic Actuators (SEA). This series-elastic actuator concept introduces an elastic element between the load and the hydraulic actuator (Robinson and Pratt 2000), as shown in Fig. 8. The elastic element decouples actuator output from the load, which provides both less mechanical impedance caused by the decrease of inertia and friction in the mechanisms, as well as greater resistance to impact loads and vibration. A position sensor measures the deflection of the elastic element in series, thus providing a measurement of the force exerted on the load. By feedforward of the measured force, the force controller modifies the actuator displacement in order to adjust the exerted force on the load. This produces a significant improvement in the quality control of the actuators' force because usual noise involved in the force control of hydraulic actuators is filtered by the elastic element. As a result, increased control and precision of force and position, energy storage in the springs and increased efficiency are achieved. The antagonist actuator of the versatile test platform must be able to exert loads up to 2500 N and speeds up to 1.5 m/s.

The use of a Series Elastic Actuator as antagonistic-load actuator is a novelty in these kinds of test benches, which usually use conventional hydraulic actuators for this purpose. The role of an antagonist-load actuator is to provide constant loads to the test actuator. However, the series elastic

actuator is able to provide precision force control so it is possible to apply programmable load profiles to the test actuator, allowing to imitate the real dynamics in robot joints. In this work, the Yobotics HEA-01 has been considered because of its higher closed-loop bandwidth. Technical specifications of this antagonist actuator are listed in Table 1.

Table 1 Technical specifications of Antagonist Actuator HEA-01

Max Power output	1.5 kW
Max Force	2500/2000 N
Max Velocity	1.5 m/s
Low Force Bandwidth	50 Hz
High Force Bandwidth	22.5 Hz
Stroke	4 in
Weight	15.6 N (3.5 lbs)
Power/Weight Ratio	96 Watts/N
Operating Pressure	3000 psi
Piston Area	0.2 in ²

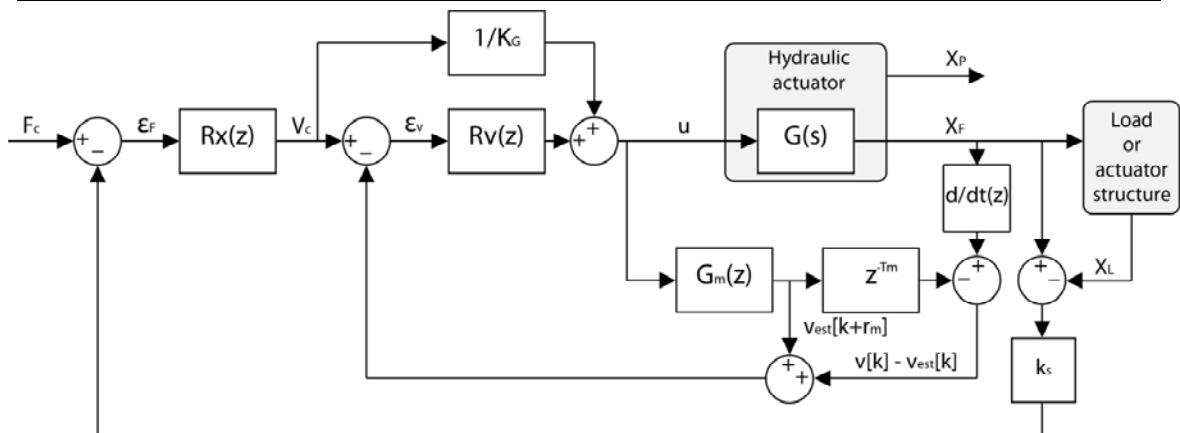


Fig. 9 Controller implemented for the antagonist actuator

In order to test and analyse actuators performance, a high-fidelity force controller has been developed for the antagonist actuator. The antagonist actuator controller has been designed to accomplish the task of reproducing the real robot dynamics as much efficiently as possible. The most important characteristic of the series-elastic antagonist actuator control scheme is that the response domain can be considered to be only velocity or position. This means that the cylinder moves the shaft with almost no dependency on the load. The implemented controller is shown in Fig. 9.

The main drawbacks of this actuator regarding its force control are the stick-slip effect and time delay. Therefore, the controller has to be able to reduce the effects of these non-linearities. To do so, the designed controller implements an inner-loop of static feed forward to deal with the actuator's stick-slip. The force settling time is reduced mainly thanks to the diminution of the stick slip effect. To deal with actuator's time delay a Smith predictor has been used. Smith predictor is needed to improve actuators force settling time, since the time delay, 4 ms, represents about 20 to

50% of the desired closed-loop settling time, explaining the need to be taken into account. Both discrete controllers $RX(z)$ and $RV(z)$ are PI controllers, and the model $Gm(z)$ used by the Smith predictor is a second order system. The achieved settling time is about 15 ms.

The antagonist actuator can be implemented in rotational configuration using a hydraulic motor and a torsional spring in series with the joint.

6. Characterization tests and benchmarking

In order to show the functionality of the proposed test platform, this section presents the experimental characterization of three actuators that are currently being used for modern legged robots: wearable robotics, prosthetics and autonomous walking robots. These actuators are:

1. Pneumatic Artificial Muscle FESTO MAS-20-200N-AA
2. Yobotics Series Elastic Actuator SEA-23-23
3. Magneto-Rheological linear damper LORD RD-1005-3

In this section, these three actuator technologies are briefly described followed by their experimental characterization. Later a comparison is presented.

6.1 Pneumatic artificial muscle

Pneumatic Artificial Muscles (PAM) are a family of biomimetic actuators, based on the McKibben Muscle, which imitate the operating principle of natural muscles (Klute and Hannafor d 2000, Kerscher *et al.* 2006). These actuators consist of a double membrane with a mesh in between, so when the air pressure increases the mesh expands radially and compresses longitudinally about 20% of its length. PAMs are currently used as antagonistic actuators for autonomous biped robots (Vanderborght *et al.* 2008), lower-limb exoskeletons for gait assistance and rehabilitation (Sawicki and Ferris 2009, Beyl *et al.* 2009), and robot hands (Komatsubara *et al.* 2009).



Fig. 10 Pneumatic Muscle FESTO MAS-20-200N-AA

Experiments on the characterization of the PAM FESTO MAS-20-200N-AA shown in Fig. 10 have been carried out using the versatile test platform in a variable load profile ranging from 6.7 to 106.7 Kg. The PAM behaviour is best characterized comparing relative contraction or strain with tensile force. In these tests, the actuator's contraction and the force were measured using the test platform's sensorial unit.

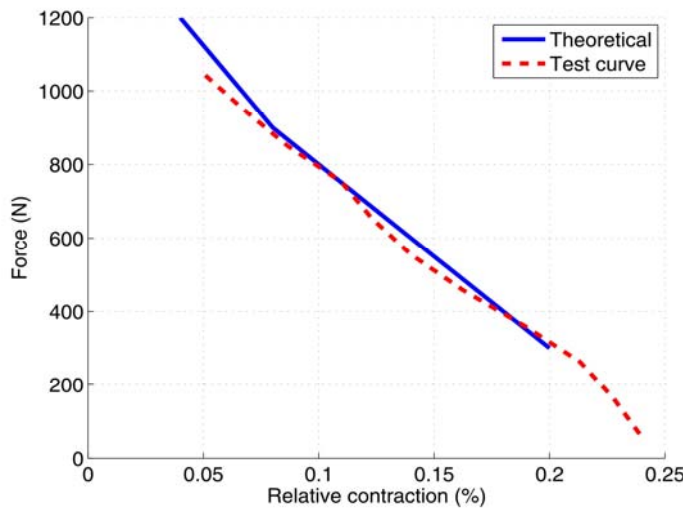


Fig. 11 FESTO MAS-20-200N-AA PAM force vs. relative contraction

Fig. 11 shows the results of the test and the theoretical curves for a 6 bar operation. As it can be seen, our experimental results obtained using the test bench correspond rather well to the theoretical behaviour.

The efficiency of the PAM was obtained using the concept of exergy efficiency instead of energy efficiency. In thermodynamics, the exergy of a system is the maximum useful work possible during a process that brings the system into equilibrium with a reservoir. Therefore, exergy is the energy that is available to be used.

In the performance evaluation of processes that use compressed air, the analysis based on the variation of internal energy is not appropriate because in these processes the internal energy is not conserved (Cai *et al.* 2002). The computation of process efficiency based on exergy as the maximum capacity to produce work is the best suited to analyze the energetic conversion efficiency. Then, exergy efficiency of the Pneumatic Muscle is the relation between work produced by the actuator (e_p) and exergy entering the system (e_e) in each working cycle

$$\eta_{II} = \frac{e_p}{e_e} \times 100(\%) \quad (1)$$

The work produced by the actuator, e_p , is the product of force and displacement measured at the load.

The maximum useful work, or exergy of the unit mass compressed air in the transition from the PAM's working pressure (6 bar) to ambient pressure (1 bar) is given by

$$e_e = (u - u_o) - T_o(s - s_o) \quad P_o(v_o - v) \quad (2)$$

where $(u - u_o)$ is the variation of internal energy of the system, $(s - s_o)$ is the variation of entropy of the system, $(v - v_o)$ is the variation in volume of the compressed air, and $T_o = 293$ K is ambient temperature and $P_o = 1$ bar is ambient pressure.

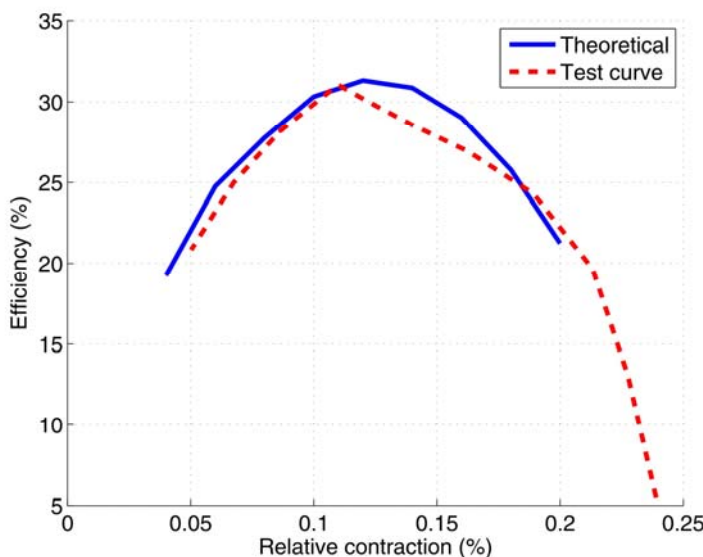


Fig. 12 FESTO MAS-20-200N-AA PAM efficiency vs. relative contraction

Fig.12 shows the actuator's efficiency vs. its relative contraction or strain. As the graph shows, the maximum measured efficiency is below 30% at 6 bar. Again there is a good correspondence between theoretical and test curves.

6.2 Series elastic actuators

Series Elastic Actuators (SEA) are a family of actuators which are specially designed for force control of robotic systems (Robinson 2000, Pratt *et al.* 2002). They introduce an elastic element in series between the load and the motor whose deflection provides a measurement of the force exerted on the load. The motor used in SEAs features good position accuracy to give a good force output. The better the motor can modulate the spring position, the cleaner the force output of the spring. Besides, the elastic element filters noise and allows for an increase in the force-controller gain within stable operation. As a whole, SEAs improve conventional actuators in force control response. This configuration also provides compliant actuation, as well as good resistance to impact and vibration. Due to their controllable adaptability to the environment, SEAs are currently

being integrated into legged robots such as biped robots (Pratt and Krupp 2008), agile quadrupeds (Garcia *et al.* 2011a) and exoskeletons (Kwa *et al.* 2009), and also they are being used in fast, soft robot arms for the safe control of human-robot interaction (Bicchi and Tonietti 2004).

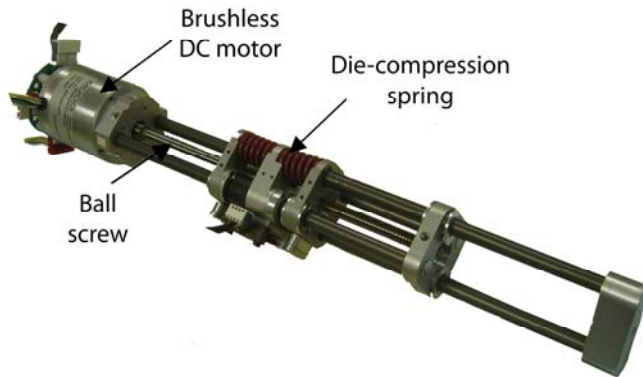


Fig. 13 Yobotics SEA 23-23

The Yobotics SEA 23-23 (see Fig. 13) was tested using the herein presented versatile test platform in a variable load ranging from 25 to 146 Kg. Figures 14 and 15 show the results of the experiments. The maximum experimental velocity, 0.27 m/s, is obtained along with the maximum efficiency, 83 %. Considering that this actuator is fairly new and there is no characteristic curve provided by manufacturers, the obtained characteristic curve in our tests can only be compared with specifications on maximum force and speed values provided by the SEAs manufacturer Yobotics Inc. which are 1300 N of maximum force at intermittent operation and maximum speed of 0.27 m/s. The experimental curve shown in Fig. 14 matches with these maximum values, and provides the complete curve for the range of forces and speeds available for this actuator. The nominal power of the actuator is 166 W in continuous operation. The experimental data shows that the actuator can deliver 200 W intermittently. It is worthwhile mentioning that this value depends on the power amplifier and therefore it could be increased slightly.

Fig. 15 shows the experimental efficiency of the actuator for the same range of speeds and forces. Again, as the SEAs manufacturer does not provide this parameter of efficiency this experimental characterization provides significant information. In order to validate the tested efficiency, it is necessary to take into consideration the combined efficiency of the elements composing the SEA. First, the efficiency of the ball screw transmission, which depends on its lead angle and friction coefficient. The ball screw used in the SEA23-23 has a theoretical efficiency of 95%. Second, the brushless DC motor in the actuator has a theoretical maximum efficiency of 90%, although this value depends on the winding resistance which changes with temperature, and the magnetic losses involving the magnetic core material, the actual motor velocity and the input current. Taking these two theoretical efficiencies into consideration, the maximum theoretical efficiency of the joint mechanism could approximate 85%. Therefore, we can state that the experimental maximum efficiency of 83% is the actual SEA 23-23 maximum efficiency.

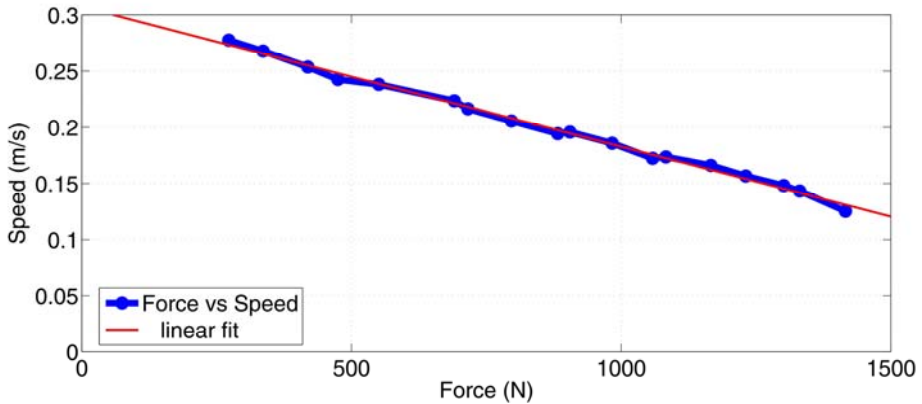


Fig. 14 Force vs Velocity curve of SEA 23-23

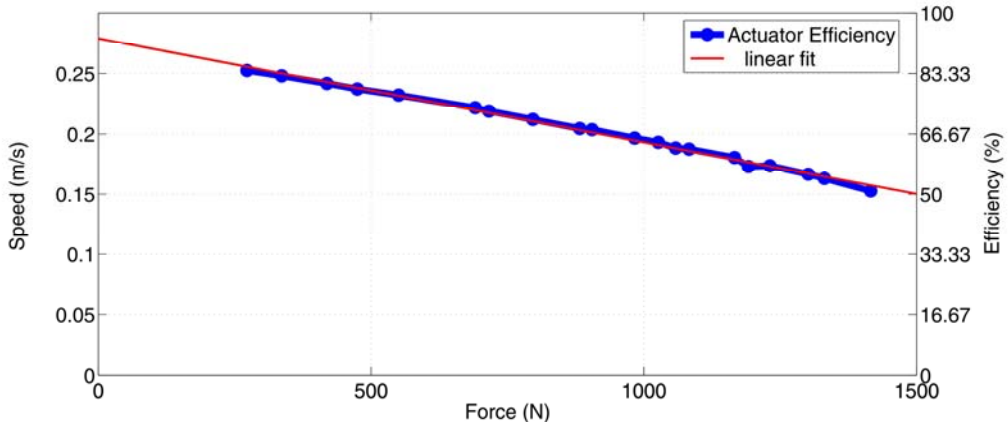


Fig. 15 Efficiency vs Velocity and Force curve of SEA 23-23

6.3 Magneto-rheological fluid dampers

Magneto-rheological fluids (MRFs) are smart materials capable of changing their apparent viscosity under the effect of a magnetic field. Taking advantage of that property, controllable dampers have been developed using these fluids (Carlson *et al.* 2004). They are resistive actuators, therefore they do not provide active movement but provide resistance to it. For this reason, MRF actuators are usually combined with other types of actuators which provide active motion, either natural (human muscle) or artificial. MRF dampers have an ability to provide high resistive torque and low additional inertia and therefore they have great potential to be used in the design of rehabilitation robots (Walsh and Endo 2007) and prosthesis (Au *et al.* 2007) and there is also significant research on haptic applications (Cassar and Saliba 2010).

The linear MRF damper shown in Fig. 16 manufactured by Lord Corporation RD-1005-3 has been tested and characterized using the versatile test bench. The RD-1005-3 is controlled by Lord's wonder box device which is commanded by a 0 to 5 Vdc voltage input signal which is converted

by the wonder box device to the damper's input current ranging from 0 to 2 A.

During the RD-1005-3 characterization tests the damper's compression and the resistive force were measured using the test bench's sensorial unit. The damper input current was measured with a current transducer LEM HY5P, and the damper supply voltage was measured using a RC low-pass filter and the platform's data acquisition system.



Fig. 16 Lord RD-1005-3 MR Linear Damper

Fig. 17 shows the results of this test. For each applied current there is a linear dependency between the exerted force and the actuator's velocity. As expected, the slope is nearly the same in each curve, but a current dependant offset is observed. For currents higher than 1.5 A the actuator saturates and the curves are practically invariant. The experimental force-speed curves show that these MRF dampers provide a linear increase of the resistive force as long as the piston speed increases for a given activation current, and that by increasing the activation current the force at rest is increased.

The power consumption measurements allowed us to confirm that it is only a function of the damper's input current, being independent of the actual load and varying from 2 W for 0 A to 15 W for 1.5 A. That is because the power consumed by the actuator is just the one needed to change the fluid's properties and maintain them.

Also, a "blocked load" operating mode has been experimentally tested. This is better observed in figure 18. It shows actuator efficiency for low speed operating points, $v < 0.008$ m/s. In this curve both actuator operating modes can be observed: "blocked load" ($v < 0.002$ m/s) and "moving load". At "blocked load" damper efficiency is ranging between 25% and 50%. Values over 100 % efficiency are achieved at "moving load" even at low operating speeds, since the dissipated power increases sharply with load speed. These experimental efficiency curves are meant to show the damping efficiency of the device, not the efficiency at creating movement. Please note that these devices are used to create a controllable resistive action, and therefore they are efficient if they are able to break the motion at a minimum power consumption.

The obtained MRF damper characterization cannot be compared with the manufacturer's specifications because none of this relevant information is provided. Only maximum damping force (2200 N) is specified. Hence, the characteristics of the damper cannot be inferred from the manufacturers' data and the use of a test platform is needed for the characterization of the device.

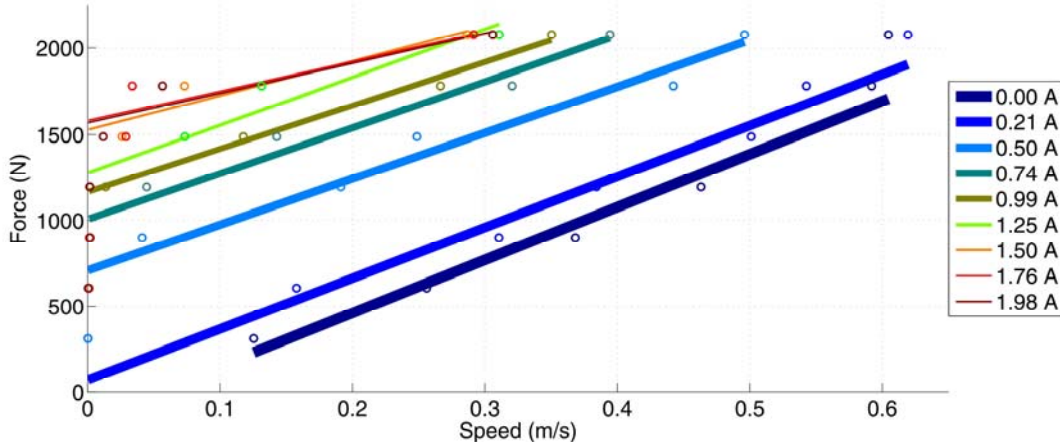


Fig. 17 MRF damper RD-1005-3 force vs velocity curves for different activation currents. Dots represent experimental data lines are linear fit

6.4 Comparative analysis of actuator performance

Table 2 compares experimental characteristic data of the three tested actuators. The first row lists actuator weight not considering power supply and other overhead material, while the second row estimates the whole weight required for the autonomous operation of the actuator in a mobile robotic system, encompassing power supply, amplifiers, valves and distribution lines where needed. Specific power and specific force values are computed (1) considering only the actuator weight and (2) considering the total weight. The settling time is the time required for the actuator to reach the reference command. The settling time of the SEA has been obtained under force control.

Among the tested active actuators the most powerful and efficient is the SEA, since it can deliver moderate power with relatively high efficiency (83%). Electric SEAs can maintain efficient behaviour in a variety of operating conditions. Conversely, the PAM can only reach a 30% efficiency at its maximum power.

Regarding the efficiency of actuators it is important to note that the SEA and the MRD results have been obtained by considering the efficiency of the whole actuator-controller-amplifier system, excluding the battery, while the results for the PAM do not include the efficiency of the compressor which introduces additional energy losses not considered here. The compressor weight also directly affects the power-to-weight and force-to-weight ratios of the PAM, and in these magnitudes the tested PAM cannot compete with those of the electrical SEA as shown in Table 2.

However, considering active and resistive actuators, MRF devices outcome the others in most parameters: power, force and efficiency, although it cannot deliver power, but dissipate it. The efficiency of an MRF damper is almost infinite, as its force-speed characteristic increases linearly for a constant power consumption. This property is worth considering when designing efficient legged robots. From the above analysis the combination SEA - MRD could be considered as a powerful and efficient choice for the joints of legged robots.

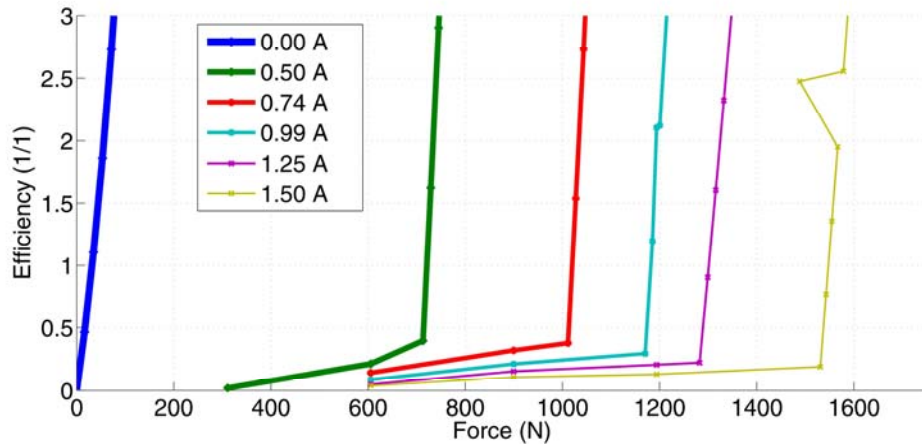


Fig. 18 MRD RD-1005-3 efficiency vs. force for different activation currents

Table 2. Experimental comparison of characteristic data of the tested actuator technologies

	MAS-20-200N-AA	SEA-23-23	RD-1005-3
Actuator Weight (kg)	1.31	1.36	0.8
Total Weight (kg)	28.3	12.86	5.2
Actuator length (mm)	443	305	208
Max. Force (N)	1040	1300	2100
Max. Power (W)	120	200	1000
Specific power (1) (W/kg)	91.6	147	1250
Specific power (2) (W/kg)	4.24	15.55	192.3
Specific force (1) (N/kg)	794	956	2625
Specific force (2) (N/kg)	36.7	101	403.8
Strain (%)	20	28.7	24
Efficiency (%)	30	83	inf
Settling time (ms)	750	2.5	15
Strain rate (Hz)	1	15.4	6

7. Conclusions

This paper presents the conceptual and mechanical design of a modular and versatile test platform for the characterization and benchmarking of specific actuators which are being recently incorporated into modern robots. These actuators for robots are frequently designed and developed by researchers and, when commercially available, they are not completely characterized, providing only nominal values of operation. Besides, actuator specifications rely on average behaviour usually analyzed for continuous operation modes with constant loading. These test conditions do not match the real operating conditions of actuators for robots. Actuators used in modern robots are subjected to highly dynamic cyclic motions. The roboticist is usually exposed to uncertainty when selecting the proper actuation system for a certain robot, because specifications, when

available, are not adequate enough to make a good selection. The use of new actuator technologies and the ever increasing dynamic-exigent use of actuator technologies makes the availability of a common platform for their characterization, test, and comparative analysis necessary.

The herein presented test platform allows the roboticist to evaluate and characterize different types of actuators, reproducing their real operational conditions. The proposed design has the following characteristics: It is modular and reconfigurable in four operational modes to fit different actuator types; It can test linear and rotational actuators of different sizes, shapes and functions, as well as different loads, powers and displacement capacities, hence providing the desired versatility; It reproduces the real kinematic and dynamic conditions which actuators used in service robotics will be exposed to by transmitting the mechanical power to a central rotational axis and by using a programmable Series Elastic Hydraulic Actuator as antagonist load; With the proposed arrangement and configuration of the elements the user can comfortably visualise the actuators' performance, and it also allows for easy installation and dismantling; A sensorial unit captures all of the variables needed to characterise the actuator to be tested; A powerful data acquisition system and a graphical user interface complete the platform with which the operational conditions can be controlled and the actuator measured signals can be monitored in real time. It provides tabular data storage for later evaluation and handling.

The performance of the proposed test platform has been demonstrated by the characterization of three controllable-impedance actuators using the test bench in its linear-linear operational mode. A Pneumatic Artificial Muscle by FESTO, a Series Elastic Actuator by Yobotics Inc. and a Magneto-Rheological Fluid Linear Damper by Lord Corp. have been characterized and finally compared, having provided a useful table with performance data for the safe selection of actuators. These experiments validate the usefulness of the versatile test platform here presented.

The modular and versatile platform for benchmarking of modern actuators for robots has been patented (Garcia *et al.* 2009b). However its replication is permitted and encouraged for non-commercial scientific purposes, always under supervision of CSIC as owner of this patent. The full patent text as well as manufacturing schematics are available on request to this paper's corresponding author.

Acknowledgements

This work has been partially funded by the Spanish Ministry for Economy and Competitiveness through grant DPI2010-18702 which has funded personnel costs and by AECID through grant PCI-iberoamerica A1/039883/11 which has funded equipment and consumable costs.

References

- Anderson, E.H., Bales, G.L. and White, E.V. (2003), "Application of smart material-hydraulic actuators", *Proceedings of the SPIE Industrial and Commercial Applications of Smart Structures and Materials*, volume 5054, 73-84, Mountain View, CA.
- Au, S.K., Weber, J. and Herr, H. (2007), "Biomechanical design of a powered ankle-foot prosthesis", *Proceedings of the 2007 IEEE 10th International Conference on Rehabilitation Robotics*, 298-304, Noordwijk, The Netherlands.
- Bar-Cohen,Y. (2000), "Electroactive polymers as artificial muscles -capabilities, potentials and challenges", In Osada, editor, *Handbook on Biomimetics*, chapter 8, sec. 11, 299-342. NTS Inc.

- Beyl, P., VanDamme, M., VanHam, R., Vanderborght, B. and Lefeber, D. (2009), "Design and control of a lower limb exoskeleton for robot-assisted gait training", *Applied Bionics and Biomechanics: special issue on lower and upper limb exoskeletons*, 6, 229-243.
- Bicchi, A. and Tonietti, G. (2004), "Fast and soft arm tactics: Dealing with the safetyperformance trade-off in robot arms design and control", *IEEE Robot Autom. Mag.*, **11**(2), 22-33.
- Cai, M., Kaaawa, T. and Kawashima, K. (2002), "Energy conversion mechanics and power evaluation of compressible fluid in pneumatic actuator systems", *Proceedings of the 37th Intersociety Energy Conversion Engineering Conference*, 438 - 443, April 24-28, 2000, San Francisco, CA, USA.
- Carlson, D., Catanzarite, D. and St. Clair, K. (2004), "Commercial magneto-rheological fluid devices", *Proceedings of the ACTUATOR 2004*, Bremen, Germany.
- Cassar, D.J. and Saliba, M.A. (2010), "A force feedback glove based on magneto-rheological fluid: Prototype development and evaluation", *Proceedings of the 1st International Conference on Applied Bionics and Biomechanics*.
- Catalano, M., Schiavi, R. and Bicchi, A. (2010). "Mechanism design for variable stiffness actuation based on enumeration and analysis of performance", *Proceedings of the IEEE International Conference on Robotics and Automation*, 3285-3291, Anchorage, AK.
- Çilingir, H.D. and Papila, M. (2010), "Equivalent" electromechanical coefficient for IPMC actuator design based on equivalent bimorph beam theory", *Experiment. Mech.*, **50**(8), 1157-1168.
- Garcia, E., Jimenez, M., Gonzalez de Santos, P. and Armada, M. (2007), "The evolution of robotics research: From industrial robotics to field and service robotics", *IEEE Robot Autom. Mag.*, **14**(1), 90-03.
- Garcia, E., Montes, H. and Gonzalez de Santos, P. (2009a), "Emerging actuators for agile locomotion", *Proceedings of the International Conference on Climbing and Walking Robots*, Istanbul, Turkey.
- Garcia, E., Sarria, J.F., Gonzalez-de-Santos, P. and Pestana, J. (2009b), Universal testbench for evaluation of actuators (In Spanish). Spanish National Research Council, CSIC. Patent ESP200931237.
- Garcia, E., Arevalo, J., Muñoz, G. and Gonzalez-de-Santos, P. (2011a), "Combining series-elastic actuation and magneto-rheological damping for the control of agile locomotion", *Robot. Auton. Syst.*, **59**(10), 827-839.
- Garcia, E., Arevalo, J., Sanchez, F., Sarria, J. and Gonzalez de Santos, P. (2011b), "Design and development of a biomimetic leg using hybrid actuators", *Proceedings of the IEEE/RSJ International Conference on Intelligent Robots and Systems*, San Francisco, CA, USA.
- Van Ham, R., Sugar, T.G., Vanderborght, B., Hollander, K.W. and Lefeber, D. (2009), "Compliant actuator designs", *IEEE Robot. Autom. Mag.*, **16**(3), 81-94.
- Hurst, J., Chestnutt, J. and Rizzi, A. (2010), "The actuator with mechanically adjustable series compliance", *IEEE T. Robot.*, **26**(4), 597-606.
- Kerscher, T., Albiez, J., Zoellner, J. and Dillmann, R. (2006), "Biomechanical inspired control for elastic legs", *Proceedings of the 9th International Conference on Climbing and Walking Robots*, Brussels, Belgium.
- Klute, G.K. and Hannaford, B. (2000), "Accounting for elastic energy storage in McKibben artificial muscle actuators", *ASME J. Dyn. Syst. Meas. Control*, **122**(2), 386-388.
- Komatsubara, H., Tsujiuchi, N., Koizumi,T., Kan, H., Nakamura, Y. and Hirano, M. (2009), "Development and control of master-slave robot hand driven by pneumatic actuator", (Eds. H. Ulbrich and L. Ginzinger), *Motion and Vibration Control*, 201-210. Springer Netherlands.
- Kwa, H.K., Noorden, J.H., Missel, M., Craig, T., Pratt, J.E. and Neuhaus, P.D. (2009). "Development of the IHMC mobility assist exoskeleton", *Proceedings of the IEEE International Conference on Robotics and Automation*. Kobe, Japan.
- Mahfoud, J. and Der Hagopian, J. (2012), "Investigations on critical speed suppressing by using electromagnetic actuators", *Smart Struct. Syst.*, **9**(4), 303-311.
- Mavroidis, C. (2002), "Development of advanced actuators using shape memory alloys and electrorheological fluids", *Res. Nondestruct. Eval.*, **14**(1), 1-32.
- Pestana, J., Bombin, R. and Garcia, E. (2010). "Characterization of magnetic shape memory alloys (MSMA)

- oriented to periodic actuation”, *Proceedings of the 2010 International Conference and Exhibition on New Actuators and Drive Systems (ACTUATOR)*, Bremen, Germany.
- Pratt, J. and Krupp, B. (2008), “Design of a bipedal walking robot”, *Proceedings of the 2008 SPIE*, volume 6962.
- Pratt, J., Krupp, B. and Morse, C. (2002), “Series elastic actuators for high fidelity force control”, *Industrial Robot. Int. J.*, **29**(3), 234-241.
- PTC (2007), *Getting started with Pro/Engineer Wildfire 4.0*, Parametric Technology Corporation, Needham, MA., USA.
- Robinson, D.W. (2000), *Design and analysis of series elasticity in closed-loop actuator force control*, Ph.D. thesis, Massachusetts Institute of Technology, Cambridge, Massachusetts, USA.
- Robinson, D.W. and Pratt, G.A. (2000), “Force controllable hydro-elastic actuator”, *Proceedings of the IEEE International Conference on Robotics and Automation*, April 24-28, 2000, San Francisco, CA, USA.
- Sawicki, G.S. and Ferris, D.P. (2009), “A pneumatically powered knee-ankle-foot orthosis (KAFO) with myoelectric activation and inhibition”, *J. Neuroengineering Rehab.*, **6**(1), 23-39.
- Song, G., Ma, N., Li, L., Penney, N., Barr, T., Lee, H.J. and Arnold, S. (2011), “Design and control of a proof-of-concept active jet engine intake using shape memory alloy actuators”, *Smart Struct. Syst.*, **7**(1), 1-13.
- Suorsa, I., Tellinen, J., Pagounis, E., Aaltio, I. and Ullakko, K. (2006), “Applications of magnetic shape memory actuators”, *Proceedings of the ACTUATOR 2006*, Bremen, Germany.
- Testek Inc. (2011), “Aircraft/Aerospace Electromechanical actuator test equipment”, Online: [http://www.parkerdenisonpk.com/hydraulic test stand/Electro Mechanical.pdf](http://www.parkerdenisonpk.com/hydraulic%20test%20stand/Electro%20Mechanical.pdf).
- Vanderborght, B., Verrelst, B., Van Ham, R., Van Damme, M., Lefeber, D., Meira Y Duran, B. and Beyl, P. (2006), “Exploiting natural dynamics to reduce energy consumption by controlling the compliance of soft actuators”, *Int. J. Robot. Res.*, **25**(4), 343-358.
- Vanderborght, B., Van Ham, R., Verrelst, B., Van Damme, M. and Lefeber, D. (2008), “Overview of the Lucy project: Dynamic stabilization of a biped powered by pneumatic artificial muscles”, *Adv. Robotics*, **22**(10), 1027-1051.
- Walsh, C.J. and Endo, K. (2007), “A quasi-passive leg exoskeleton for load-carrying augmentation”, *Int. J. Humanoid Robotics (IJHR)*, 4.

Appendix

A. Equations of motion for test actuators

The test platform provides torque and speed measured by the sensorial unit located at the central axis of the bench. From these measurements, the magnitudes of force and speed of the test actuators are obtained making use of the following equations of motion.

A.1 Dynamic equations for linear actuators

The force generated by the linear test actuator is computed making use of the free body diagram shown in Fig. 19, and applying Newton's second law. The following derivation of equations of motion is based on the nomenclature listed in Table 3.

Table 3 Nomenclature for deriving the equations of motion

\vec{F}_a	Force exerted by the linear actuator
$\vec{\tau}_s$	Torque measured by the torque sensor
$\vec{\tau}_f$	Friction torque generated by contact between the central axis and the bushings
\vec{W}_{cr}	Weight of the connecting rod
$\ddot{\alpha}$	Angular acceleration of the axis, read by the torque sensor
$\dot{\omega}$	Angular velocity of the axis, read by the torque sensor
λ	Linear actuator's lead angle relative to the horizontal plane
θ	Angular position of the connecting rod measured by the sensorial unit with origin in the vertical plane
$I_{xx_{ec}}$	Moment of inertia along the axis x of the bellows coupling (provided by manufacturer)
$I_{xx_{cr}}$	Moment of inertia along the axis x of the "connecting rod - central axis" system (calculated with Pro-engineer)

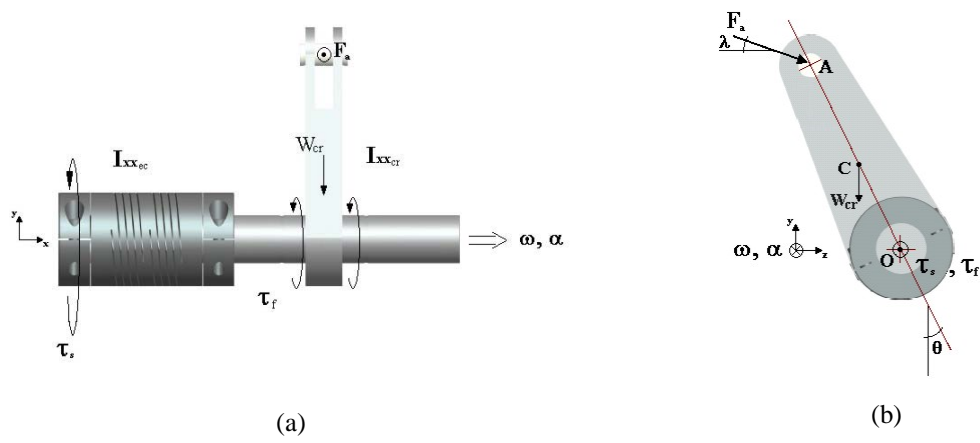


Fig. 19 Free body diagram of the "central axis - connecting rod - bellows coupling" system

A summation of the momentum in point O results in

$$\vec{r}_{OA} \times \vec{F}_a + \vec{r}_{OC} \times \vec{W}_{cr} + \vec{\tau}_s + \vec{\tau}_f = (I_{xx_{ec}} + I_{xx_{cr}}) \vec{\alpha} \quad (3)$$

where \vec{r}_{OA} is the position vector of the point A where the actuator force is applied, relative to point O, which is computed as

$$\vec{r}_{OA} = d_{OA} [\cos(\theta) \vec{j} - \sin(\theta) \vec{k}] \quad (4)$$

being d_{OA} the distance between points O and A. The force vector of the actuator is defined as:

$$\vec{F}_a = F_a [\cos(\lambda) \vec{k} - \sin(\lambda) \vec{j}] \quad (5)$$

Determining the cross product of \vec{r}_{OA} and \vec{F}_a

$$\vec{r}_{OA} \times \vec{F}_a = | \vec{F}_a | d_{OA} \cos(\lambda + \theta) \vec{i} \quad (6)$$

The weight of the connecting rod is defined as

$$\vec{W}_{cr} = -M_{cr} g \vec{j} \quad (7)$$

where M_{cr} is the mass of the connecting rod and $g=9.8 \text{ m/s}^2$ is gravity acceleration.

The term \vec{r}_{OC} in Eq. (3) is the position vector of the connecting rod's center of mass (point C) in relative to point O, which has the form

$$\vec{r}_{OC} = d_{OC} [\cos(\theta) \vec{j} - \sin(\theta) \vec{k}] \quad (8)$$

Now determining the cross product of \vec{r}_{OC} and \vec{W}_{cr}

$$\vec{r}_{OC} \times \vec{W}_{cr} = -M_{cr} g d_{OC} \sin(\theta) \vec{i} \quad (9)$$

Taking into consideration that $\vec{\tau}_s = -\tau_s \vec{i}$, $\vec{\tau}_f = -\tau_f \vec{i}$ and $\vec{\alpha} = \alpha \vec{i}$ and substituting Eqs. (6) and (9) into (3) the following expression for the amount of force exerted by the actuator is found

$$F_a = \frac{(I_{xx_{ec}} + I_{xx_{cr}}) \alpha + M_{cr} g d_{OC} + \tau_s + \tau_f}{d_{OA} \cos(\lambda + \theta)} \quad (10)$$

It is important to bear in mind that these equations do not take the mass of the linear actuator

into account.

A.2 Kinematic equations for linear actuators

Let us consider the kinematic model of the “linear actuator - connecting rod - central axis” system shown in Fig. 20, where r represents the stroke and $l_1 + l_2$ corresponds to the actuator’s length in its maximum compression, that is, when the stroke has the minimum value.

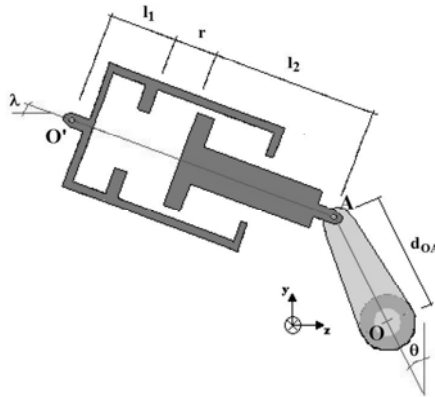


Fig. 20 Kinematic model for “linear actuator - connecting rod - central axis” system

The following equations relate the angular position of the central axis (θ), given by the sensorial unit, with the linear actuator’s stroke (r) and actuation angle (λ).

$$\dot{\theta}d_{OA} \sin \theta = \dot{\lambda}(l_1 + r + l_2) \cos \lambda + \dot{r} \sin \lambda \quad (11)$$

$$\dot{\theta}d_{OA} \cos \theta = \dot{\lambda}(l_1 + r + l_2) \sin \lambda - \dot{r} \cos \lambda \quad (12)$$

Solving for the actuator stroke (r) and actuator speed (\dot{r})

$$r = \frac{\dot{\theta}d_{OA}(\sin \theta + \cos \theta \tan \lambda)}{\dot{\lambda}(1 + \tan \lambda)} - (l_1 + l_2) \quad (13)$$

$$\dot{r} = \sqrt{\dot{\theta}^2 d_{OA}^2 + 2\dot{\lambda}^2(l_1 + r + l_2)^2 - 2\dot{\theta}\dot{\lambda}d_{OA}(l_1 + r + l_2)(\sin \theta + \cos \theta)} \quad (14)$$

A.3 Dynamic equations for rotational actuators

In order to calculate the torque generated by a rotational test actuator (τ_a) making use of the

torque measurement at the sensorial unit (τ_s), the free body diagram of Fig. 21 is used, following the same notation listed in Table 3 and being $I_{xx_{ecs}}$ the moment of inertia along the axis x of the bellows coupling on the sensor side and $I_{xx_{eca}}$ the moment of inertia along the axis x of the bellows coupling on the test actuator side.

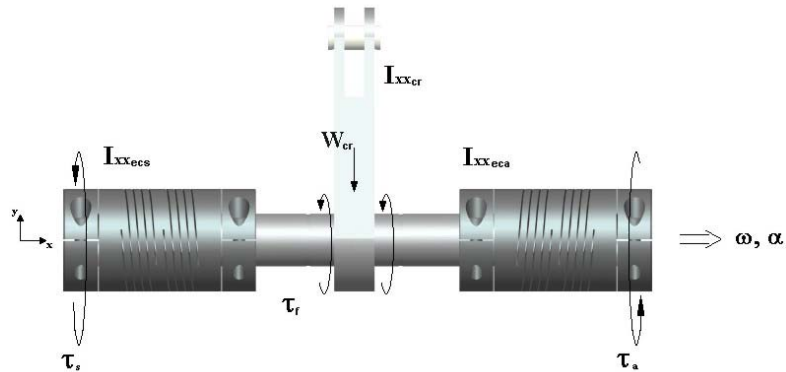


Fig. 21 Free body diagram of the “bellows coupling - central axis - bellows coupling” system used in the attachment of rotational actuators

A summation of momentum on any point on the x axis results in

$$\vec{\tau}_a + \vec{\tau}_s + \vec{r}_{OC} \times \vec{W}_{cr} + \vec{\tau}_f = (I_{xx_{ecs}} + I_{xx_{cr}} + I_{xx_{eca}}) \vec{\alpha} \quad (15)$$

The magnitude of the torque exerted by the actuator is computed from the previous equation as

$$\tau_a = (I_{xx_{ecs}} + I_{xx_{cr}} + I_{xx_{eca}}) \alpha + \tau_s + \tau_f \quad (16)$$